CANCER
CYTOPATHOLOGY

Evidence of Intrinsic Differences in the Light Scattering Properties of Tumorigenic and Nontumorigenic Cells

Judith R. Mourant, Ph.D.[1]
Andreas H. Hielscher, Ph.D.[1]
Angelia A. Eick, B.S.[1]
Tamara M. Johnson, A.D.[1]
James P. Freyer, Ph.D.[2]

[1] Bioscience and Biotechnology Group, Chemical Sciences and Technology Division, Los Alamos National Laboratory, Los Alamos, New Mexico.

[2] Molecular and Cellular Biology Group, Life Sciences Division, Los Alamos National Laboratory, Los Alamos, New Mexico.

Presented at the following meetings: Advances in Optical Technologies for Medicine and Surgery, Snowbird, Utah, July 16, 1997; Optical Society of America Conference, Long Beach, California, October 12–17, 1997; SPIE Conference BiOS '98 San Jose, California, January 26, 1998; and the Gordon Research Conference: Lasers in Medicine and Biology, New Hampshire, June 14–19, 1998.

The authors greatly appreciate the technical assistance of Dan Shen in preparing some of the cells suspensions that were measured.

Financial support from NIH Grants 1RO1CA71898 and 1RO1ES07845. Dr. Andreas Hielscher also received support through the Los Alamos National Laboratory postdoctoral fellowship program and Angelia Eick received support through the undergraduate research semester program at Los Alamos National Laboratory.

Dr. Hielscher's current address: Department of Pathology, State University of New York Health Science Center, Box 25, 450 Clarkson Avenue, Brooklyn, NY 11203.

Address for reprints: Judith R. Mourant, Ph.D., MS E535, Los Alamos National Laboratory, Los Alamos, NM 87545.

Received March 20, 1998; revision received July 9, 1998; accepted July 21, 1998.

BACKGROUND. The objective of this study was to determine whether there are intrinsic differences in the light scattering properties of tumorigenic and nontumorigenic cells from a multistep carcinogenesis model.

METHODS. Wavelength-dependent and polarization-dependent light scattering properties of cell suspensions were measured.

RESULTS. Statistically significant differences were found between the tumorigenic and nontumorigenic cells.

CONCLUSIONS. Differences in the light scattering properties of tumorigenic and nontumorigenic cells are attributed to a change in the average size of the scattering centers on the order of a few ten of nanometers. This work is relevant to the development of noninvasive optical methods for cancer diagnosis. ***Cancer (Cancer Cytopathol)* 1998;84:366–74.** © *1998 American Cancer Society.*

KEYWORDS: cancer diagnosis, light scattering, turbid media, tumorigenesis models.

Optical techniques for cancer diagnosis currently are being developed that offer significant advantages over standard techniques such as tissue biopsy.[1,2] Optical techniques are faster, sedatives are not needed, and complications associated with tissue removal (e.g., infection) are eliminated. Initial in vivo work in this area has shown that differences in optical signals such as fluorescence,[3–5] elastic-scatter[6–8] photon migration,[9] and potentially optical coherence tomography[10] can be correlated with malignancy. However, to our knowledge there has been very little research conducted to understand the underlying causes of these correlations, particularly for scattering properties. In this article we begin to address the question of whether there are intrinsic differences in the scattering properties of tumorigenic and nontumorigenic cells by determining the optical properties of cells from different stages of an in vitro tumorigenesis model.

Tissue is a highly scattering medium. At the majority of wavelengths, the probability of light scattering is significantly higher than the probability of light being absorbed (Fig. 1). The average distance before scattering events typically is in the range of 0.02–0.005 cm, depending on tissue characteristics.[11] The average distance between absorption events is > 0.2 cm in the infrared, but can be as small as 0.001 cm where the absorption of blood peaks in the visible.[12] Tissue properties are reported in terms of the scattering coefficient, μ_s, which is the inverse of the average distance between scattering events, and the absorption coefficient, μ_a, which is the inverse of the average distance a photon travels before being absorbed. In addition

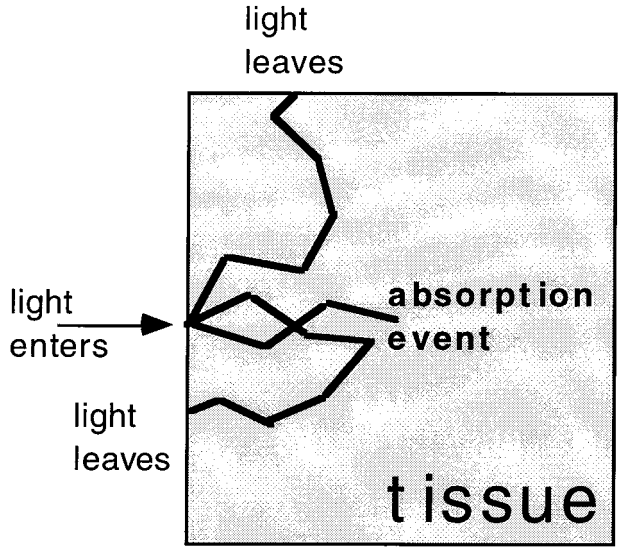

FIGURE 1. Schematic diagram of light transport in tissue. Examples are shown of paths through the tissue that the light can take. One absorption event is denoted. The scattering events, which far outnumber the absorption events, usually change the direction of light propagation by < 90 degrees.

light transport through tissue is dependent on the angles by which the light is scattered. The probability of scatter through an angle theta is referred to as $P(\theta)$ and is called the phase function. The average of the cosine of the scattering angle, $g = \int P(\theta)\cos\theta d\Omega$, is a measure of forward scattering. For a highly forward scattering media g is near 1, whereas for isotropic scattering $g = 0$. For tissue g is approximately 0.9. A reduced scattering coefficient, $\mu_s' = \mu_s(1\text{-}g)$ (which adjusts the scattering coefficient according to the amount of forward scatter) also is frequently used for characterizing tissue scattering. The reduced scattering coefficient is very similar to a person's intuitive idea of how scattering a medium is. If something appears highly scattering (like whole milk) it will have a large value of μ_s' and if something appears less scattering (like skim milk) it will have a smaller value for μ_s'.

All the tissue properties discussed earlier are wavelength-dependent properties. The wavelength dependence of light scattering is sensitive to the morphology of light scatterers and is one of the properties reported in this article. Another important property of light is its polarization (i.e., the direction(s) in which the electric field points with respect to the direction of propagation of the light). If the light is propagating in the z-direction and the electric field oscillates along the x axis, then the light is linearly polarized. Another example of linear polarization is to have the electric field oscillating along the y axis. These two examples of linear polarization are perpendicular to each other. Light also can be polarized circularly. In this case the direction of oscillation of the electric field changes with time. For example, if the electric field initially is pointed along the positive x axis, it will rotate to point along the y axis and then along the negative x axis, eventually completing the circle along the positive x axis again. There are two directions in which the rotation can occur and these are referred to as left and right circularly polarized light. Light scattering will change the polarization of the light and this change will depend on properties of the scatterers. In this article results of measurements of changes in polarization due to interaction with biologic cells are reported.

MATERIALS AND METHODS

Cell Culture

The M1 and MR1 cell lines were used as an in vitro tumorigenesis model.[13] M1 cells are derived from normal rat embryo fibroblasts by constitutive expression of a c-*myc* oncogene; these cells are immortalized but will not form a tumor in mice. MR1 cells are derived from M1 cells by additional constitutive expression of a mutant h-*ras* oncogene; inoculation of nu/nu mice with MR1 cells results in rapid, invasive tumor growth with tumors reaching a volume > 10 cm^3 in 2 weeks.[14] Cells were grown in Dulbecco's modified Eagle medium (Gibco, Grand Island, NY) supplemented with 5% fetal bovine serum (HyClone Laboratories, Inc., Logan, UT), D-glucose (4.5 mM), and antibiotics (penicillin/streptomycin). Cells were maintained in monolayer culture as explained elsewhere.[15] For these experiments, cells were inoculated into 850-cm^2 roller bottles containing 200 mL of complete medium equilibrated with a gas phase of 5% CO_2/95% air and cultured for 4 days at 37 °C using a standard roller apparatus. Due to problems with cell detachment in roller bottles at high density, plateau phase MR1 cells were cultured in 150-cm^2 tissue culture flasks containing 50 mL of complete medium in a humidified 37 °C incubator equilibrated with 5% CO_2/95% air. Exponential phase cells were inoculated such that the cell number was $< 5 \times 10^4$ (M1) or $< 2 \times 10^5$ (MR1) cells per cm^2 at harvesting; plateau phase cultures were inoculated such that the cell number was $> 2 \times 10^5$ (M1) or $> 8 \times 10^5$ (MR1) cells/cm^2 at harvesting. Growth curves demonstrated that cells in exponential phase cultures essentially were comprised of 100% proliferating cells, whereas plateau phase cultures had $< 10\%$ proliferating cells. Variation in cell number per cm^2 culture surface area for a given culture condition was $< 10\%$ for all experiments. Cells were harvested by exposure to 0.25% trypsin (Sigma Chemical Co., St Louis, MO) for 10 minutes followed by the addition of an equal

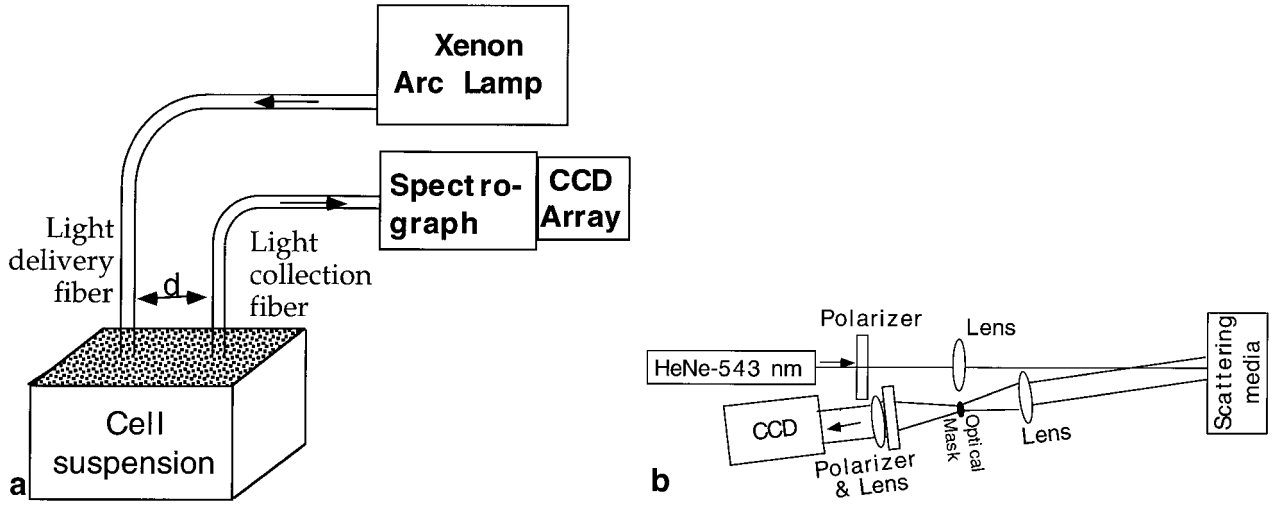

FIGURE 2. (a) Schematic diagram of the system used to measure the elastic-scatter signal, the reduced scattering coefficient, $\mu_s'(\lambda)$, and the absorption coefficient, $\mu_a(\lambda)$. Optical fibers are used to deliver the light from the lamp to the cell suspension and to collect light that has been scattered from the cells. (Arrows show the direction of light travel.) The collected light then is spectrally dispersed so that intensity can be determined as a function of wavelength. For measurements of the elastic-scatter signal, d was set at 550 μm and the 2 fibers were bundled together. For the measurements of $\mu_s'(\lambda)$ and $\mu_a(\lambda)$, several fiber separations were used as described in the text. CCD: (b) Schematic diagram of the polarization sensitive diffuse backscattering system. Arrows show the direction of light travel. Light from a green (rather than the common red) helium-neon laser is incident on the suspension of cells. Light from around the point of incidence of the laser beam then is focused onto the CCD. (The specular reflection of the incident laser beam is blocked.) nm: nanometer.

volume of ice-cold complete medium. Cell suspensions were passed through an 18-gauge needle to obtain a single cell suspension, centrifuged (1000 g $\times$ 10 minutes), resuspended in ice-cold calcium free and magnesium free phosphate-buffered saline (PBS) (Gibco), centrifuged again, and resuspended in ice-cold PBS at a concentration of 1 $\times 10^8$ cells/mm. Cell suspensions were kept on ice until (and in some cases during) optical analysis.

Cell Counting and Volume Analysis

An aliquot of each cell suspension was counted using an electronic particle counter (Coulter Electronics, Hialeah, FL) interfaced to a pulse-height analyzer (Nucleus, Inc., Oak Ridge, TN). Three replicate counts were made of each suspension and averaged. During counting, a cell volume distribution was accumulated using the pulse-height analyzer; all counts were corrected for the presence of low volume acellular debris. Cell volume distributions of $>$ 10,000 events were transferred to a computer (Macintosh; Apple Computers, Cupertino, CA) and analyzed to determine a mean cell volume as calibrated against different sizes of polystyrene microspheres.

Elastic-Scatter Measurements

Cells were placed in an open-topped measurement chamber at a concentration of 10^8 cells/mL. Light from a Xenon arc lamp was incident on the cell suspension through a 400-μm optical fiber and light was collected with a 200-μm fiber spaced 550 μm away (center-to-center). The light was dispersed spectrally to make wavelength-dependent measurements with an Acton 275i Spectrograph (Acton, Research Corp, Acton, MA). Light detection was performed by a thermoelectrically cooled Princeton Instruments (Princeton, NJ) CCD array. Data was obtained over the wavelength range 345–800 nanometers (nm). A spectrum of a material, spectralon (Labsphere Inc., North Sutton, NH), with a flat spectral response also was recorded and these data were used to correct for the wavelength dependence of the optical fibers, light source, and detector. All data presented are a ratio of the measured light intensity from the cell suspension to the measured intensity reflected from a piece of spectralon and therefore the data are unitless.

Measurement of $\mu_a(\lambda)$ and $\mu_s'(\lambda)$

Cells at a concentration of 1 $\times$ 10^8 cells/mL were placed in an open-topped measurement chamber with a depth of 3 cm, a length of 3 cm, and a width of 1.9 cm. To minimize the effects of a finite geometry, the inside was flat black. The measurement system is shown schematically in Figure 2 and is nearly identical to the one used for measuring the elastic-scatter signal. The differences are that a bigger source fiber was

used (600 μm vs. 400 μm) and that the separation between the source and detector fibers varied between 0.38–1.4 cm (rather than being set at 550 μm). Both fibers were glued into pieces of black plastic to facilitate being placed on the surface of the medium. A spectrum of a material with a flat spectral response also was recorded and used to correct for the wavelength dependence of the optical fibers, light source, and detector.

The data were analyzed according to the semiinfinite diffusion approximation.[16,17] In other words, it is assumed in the analysis that the cell suspension is infinitely deep and extends infinitely in lateral extent. This assumption can be made because the light only penetrates a short distance into the medium and therefore the measurement is not sensitive to the fact that the cell suspension is finite in extent. The purpose of making the approximation is that it makes the mathematical equations that describe the transport of light through the medium solvable. The details of data analysis are given below. One of the most important points is that despite the length and complexity of the equations there are only two variables that are varied to fit the measured data. They are the absorption coefficient, $\mu_a(\lambda)$, and the reduced scattering coefficient, $\mu_s'(\lambda)$.

Both the fluence and the flux contributions to the signal were considered. At each wavelength the light intensity was fit to the following expression:

$$I(d) = C\left\{\begin{array}{c} \mu_t'\left[\dfrac{\exp(-\mu_{eff}r_1)}{r_1} - \dfrac{\exp(-\mu_{eff}r_2)}{r_2}\right] \\ + \dfrac{1}{\mu_t'}\left(\dfrac{1}{r_1} + \mu_{eff}\right)\dfrac{\exp(-\mu_{eff}r_1)}{r_1^2} \\ + \left(\dfrac{1}{\mu_t'} + 2z_b\right)\left(\dfrac{1}{r_2} + \mu_{eff}\right)\dfrac{\exp(-\mu_{eff}r_2)}{r_2^2} \end{array}\right\} \quad (1)$$

in which

$$r_1 = \sqrt{\left(\frac{1}{\mu_t'}\right)^2 + d^2} \quad r_2 = \sqrt{\left(\frac{1}{\mu_t'} + 2z_b\right)^2 + d^2}$$

$$\mu_{eff} = \sqrt{\frac{\mu_a}{D}}, \quad \mu_t' = \mu_s' + \mu_a,$$

$$D = \frac{1}{3(\mu_s' + \mu_a)}, \quad z_b = 2AD,$$

in which A is a parameter that accounts for reflections at the surface of the cell suspension, d is the separation between the source and detector fibers, and C is an overall amplitude factor. For this work a value of 1.1 was used for A, indicating a slight mismatch of boundary conditions. Changing A to a value of 1.0 does not change the results. C is the same for all wavelengths because the data were corrected for the wavelength dependence of the source, the fibers, and the detector.

For each set of cell measurements a measurement of polystyrene spheres was performed. The constant C was determined by adjusting it so that there was a good fit between measured and theoretical values of $\mu_s'(\lambda)$ for the polystyrene sphere suspension. Therefore, the only parameters varied when fitting the cell data were $\mu_s'(\lambda)$ and $\mu_a(\lambda)$.

Polarized Diffuse Backscattering Measurements

Changes in the polarization of light due to interaction with highly scattering media have been shown to be able to differentiate turbid media.[18,19] A schematic of a system for making these polarized diffuse backscattering measurements is shown in Figure 2b. The light incident on the sample is polarized. Light that has penetrated into the sample and been scattered such that it is reemitted on the same side of the sample at which the light was incident then is analyzed with a different polarizer. Measurements can be made with various combinations of circularly and linearly polarized light to characterize the optical properties of the cell suspension. Here we are interested primarily in measurements with circular polarizers. In particular we are interested in the measurement determined from the four intensity measurements shown in Equation 2. L indicates left circularly polarized light and R indicates right circularly polarized light. The first letter of each two-letter combination is the polarization of the incident light, and the second letter is the polarization of the detected light. This measurement is denoted by M_{44}, because it is formally the M_{44} matrix element of the Mueller matrix.[20] It is a measurement of how effectively a medium flips the helicity of backscattered light. For a perfect mirror $M_{44} = -1$, because a mirror flips the helicity (i.e., the rotation direction) of the light.

$$M_{44} = (LL + RR - LR - RL)/4 \quad (2)$$

In this work, M_{44} is normalized (i.e., divided) by a measurement made with no polarizers in the beam path. This measurement is formally the M_{11} matrix element and is identical to the "video reflectometry" measurements of other authors.[21,22] The result of a measurement with no polarizers is an azimuthally symmetric image of radially decreasing intensity. The decrease in intensity is faster for more highly scattering media and slower for less scattering media. The M_{44} matrix element also is influenced by this decrease in radial intensity. Because the aim of measuring the

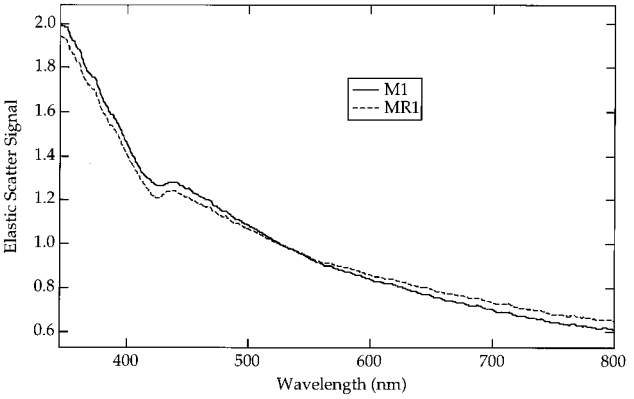

FIGURE 3. The wavelength dependence of the elastic-scatter signal from suspensions of M1 and MR1 cells (cell concentration = 10^8 cells/mL). To emphasize the difference in the wavelength dependence, the data have been normalized to have the same area from 345 nanometers (nm) to 800 nm. The cells were harvested in the exponential phase of growth.

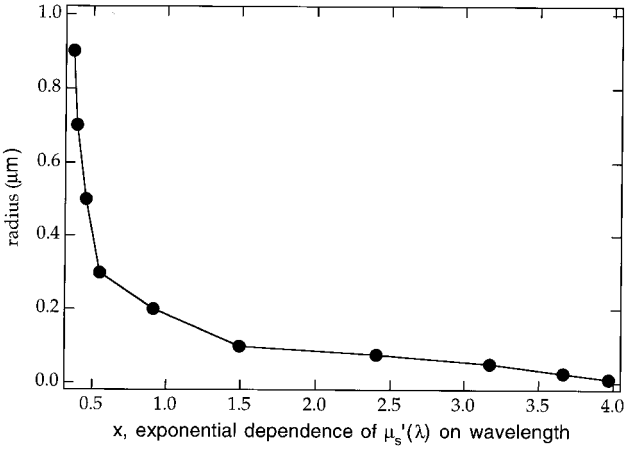

FIGURE 4. Correlation between the size of light scatterers and the wavelength dependence of the reduced scattering coefficient $\mu_s'(\lambda)$. The radius of a monodisperse distribution of spheres is plotted as a function of the power law dependence of $\mu_s'(\lambda)$ on λ. The reduced scattering coefficient for a particular size particle was fit to $c\lambda^{-x}$. In this graph, the x axis is *x* and the y axis is radius. The scatterers had an index of 1.4 and the medium had an index of 1.35.

M_{44} matrix element is to examine the interaction of the cells with polarized light, all the M_{44} measurements are divided by the M_{11} matrix element.

The M_{44} matrix elements for cell suspensions are azimuthally symmetric.[18] Therefore, the information contained in the M_{44}/M_{11} matrix element can be expressed as matrix value versus radial distance. The polarization effects are expected to be stronger for photons that have undergone less scattering events than for those that have undergone more scattering events. Therefore, to compare polarization effects of media with different scattering coefficients, the radial position is expressed in units of $1/\mu_s'$. For example, the physical distance of 0.5 cm for a medium with $1/\mu_s' = 0.25$ cm corresponds to a radial position of 2 in units of $1/\mu_s'$.

The value of μ_s' was determined from measurements with linear polarizers.[19]

RESULTS

Differences in Elastic-Scatter Signal

Figure 3 shows the wavelength dependence of the elastic-scatter signal measured for suspensions of M1 and MR1 cells harvested in the exponential phase of growth. The decrease in signal with wavelength is steeper for the M1 cells than for the MR1 cells. This experiment also has been performed for cells in the plateau phase of growth with very similar results. In all, the experiment was repeated for four sets of cells with the consistent result that the decrease in signal with wavelength is faster for the M1 cells than for the MR1 cells.

The elastic-scatter signal is a function of both the absorption and scattering properties of the medium. Changes in chromophores as well as changes in morphologic properties will affect the wavelength dependence of the collected light. The effects of absorption on the elastic-scatter signal tend to be relatively narrow dips in the spectrum. The dip at approximately 420 nm in Figure 3 is due to an absorption band. Scattering changes tend to be slower functions of wavelength. However, neither of these statements is absolute.[23]

Difference in the Wavelength Dependence of $\mu_s'(\lambda)$

To ascertain whether the difference in the elastic-scatter signal of the M1 and MR1 cells is due to a difference in the absorption or scattering properties, measurements were performed to determine the scattering and absorption properties separately. Specifically, the absorption coefficient, $\mu_a(\lambda)$, and the scattering coefficient $\mu_s'(\lambda)$, were measured in two experiments on M1 and MR1 cells harvested in the plateau phase of growth and in three experiments on M1 and MR1 cells harvested in the exponential phase of growth. In all cases the scattering decreased more rapidly as a function of wavelength for the M1 cells than for the MR1 cells.

To quantitate the differences in $\mu_s'(\lambda)$ of the M1 and MR1 cells, the $\log(\mu_s'(\lambda))$ versus $\log(\lambda)$ was fit to a straight line. This metric was chosen because it has been shown that if the wavelength dependence is parameterized as $\mu_s'(\lambda) = c\lambda^{-x}$, that particle size can be estimated from x.[24] Figure 4 shows how the radius of

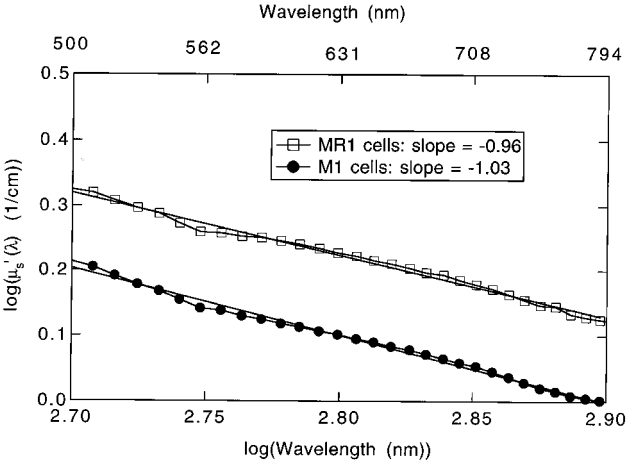

FIGURE 5. Example of the wavelength dependence of the reduced scattering coefficient, $\mu_s'(\lambda)$, for M1 and MR1 cells harvested in the exponential phase of growth. The slope is greater for the M1 cells, indicating that the light scatterers in the M1 cells are smaller than the light scatterers in the MR1 cells. nm: nanometers.

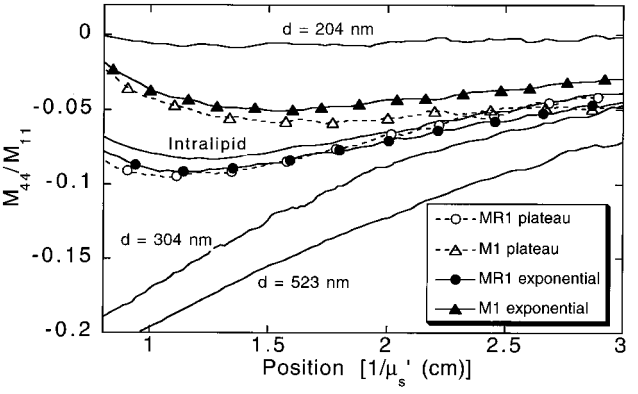

FIGURE 6. Results of measurements of light scattering performed with polarized light. The value of the M_{44}/M_{11} matrix element is shown as a function of distance from the point of laser incidence. The M_{44}/M_{11} matrix element is measured using circularly polarized light and can be associated with the size of the particles that scatter light. Results are shown for polystyrene spheres as well as for intralipid and cell suspensions. The polystyrene spheres had as dimensions 204, 304, and 523 nanometers (nm) as labeled in the figure. The curve for intralipid also is labeled. Plateau refers to cells that were harvested in the plateau phase of growth and exponential refers to cells that were harvested in the exponential phase of growth.

a monodisperse distribution of spheres is related to the power law dependence of $\mu_s'(\lambda)$ on λ.

An example of the wavelength dependence of $\mu_s'(\lambda)$ for plateau phase cells is shown in Figure 5, in which $\log(\mu_s'(\lambda))$ is plotted versus $\log \lambda$. The slopes of straight line fits to this data are -1.03 for the M1 cells and -0.96 for the MR1 cells. The dip at approximately 560 nm is due to an absorption at that wavelength and demonstrates that the diffusion approximation used in evaluating this data is not perfect. When data points in the vicinity of 560 nm are excluded the slopes of linear fits to $\log(\mu_s'(\lambda))$ versus $\log(\lambda)$ are -1.05 and -0.98, respectively. Therefore, the absolute values of the slopes are affected by the absorption but the differences in slopes are not.

The average difference in the slope of $\log(\mu_s'(\lambda))$ versus λ for pairs of M1 and MR1 cells in the same phase of growth was determined to be 0.05 with a standard deviation of 0.02. The M1 cells always had the steeper wavelength dependence as shown in the example in Figure 5. In Figure 4 it is demonstrated that a steeper wavelength dependence corresponds to smaller scatterers. Therefore, it is likely that the average scattering center is smaller in the M1 cells than in the MR1 cells. An estimate of the change in the size of the average scatterer also can be made. From our knowledge of the average slope of $\log(\mu_s'(\lambda))$ versus $\log(\lambda)$ (approximately -1.0), it is estimated from Figure 4 that the change in average scatterer radius is on the order of 10 nm.

The same measurements used to determine $\mu_s'(\lambda)$ also were used in determining $\mu_a(\lambda)$. No consistent difference was found between $\mu_a(\lambda)$ for the M1 and MR1 cells. We also noted that the amplitude observed in Figure 5 (in contrast to the difference in slope) of $\mu_s'(\lambda)$ for the M1 and MR1 cells was not found to be consistently different for all pairs of M1 and MR1 cells that were measured.

Difference in Diffuse Backscattering of Polarized Light

Examples of the radial dependencies of the M_{44}/M_{11} matrix element are shown in Figure 6. The magnitude of the M_{44}/M_{11} matrix element is larger for the MR1 cells than for the M1 cells. These measurements were repeated for four sets of cells in the exponential phase of growth and five sets of cells in the plateau phase of growth. Table 1 contains values for the M_{44}/M_{11} matrix element for M1 and MR1 cells in the exponential and plateau phase of growth. The magnitude of M_{44}/M_{11} clearly is larger for the MR1 cells than the M1 cells. (The values of M_{44}/M_{11} in Table 1 all were measured at the same distance from the point of laser incidence. This distance is equivalent to $1.2*(1/\mu_s')$ [i.e., a value of 1.2 on the x axis of Figure 6].) The M_{44}/M_{11} matrix element can be related to scatterer size. In addition to the data regarding cells, Figure 6 also shows M_{44}/M_{11} matrix elements for three sizes of polystyrene spheres and for intralipid, a fat emulsion that often is used to simulate the optical properties of tissue. The magnitude of M_{44}/M_{11} increases with increasing sphere size. Interpolating the M_{44}/M_{11} values between the 304-nm

TABLE 1
Differences in Polarized Light Scattering Properties and Apparent Dimensions of Scatterers in M1 and MR1 Cells

	M1 exponential	M1 plateau	MR1 exponential	MR1 plateau	Intralipid
M_{44}/M_{11}	−0.053 ± 0.014	−0.065 ± 0.01	−0.088 ± 0.01	−0.098 ± 0.013	−0.098 ± 0.013
Apparent scatterer dimension	236 ± 10nm	245 ± 8nm	261 ± 8nm	268 ± 10nm	257nm

nm: nanometers.

polystyrene sphere suspensions and the 204-nm polystyrene sphere suspension, one can determine apparent dimensions (d_a) for the scatterers in the cell suspensions. The results are given in Table 1. These results imply that the difference between MR1 and M1 cells is caused by a particle dimension increase of approximately 25 nm.

A striking difference between the measurements of spheres and the measurements of intralipid and cells in Figure 6 is that the M_{44}/M_{11} matrix elements are nearly linear as a function of position for the spheres, but not for the intralipid and cell suspensions. Intralipid contains a broad range of scatterer sizes with particle dimensions ranging from 25–675 nm.[25] Cells also are expected to contain a broad range of scatterers. Therefore, we expect that the difference between the form of the radial dependence of the M_{44}/M_{11} matrix elements for the spheres versus the cells and intralipid is due to the fact the sphere suspensions are comprised of a single size scatterer whereas the intralipid and cell suspensions are comprised of multiple size scatterers. Furthermore, this means that the apparent dimension represents a weighted average of the scatterers. Based on the measurement for intralipid the weighting is toward larger particles. The apparent dimension for intralipid was found to be 257 nm whereas the average dimension of a scatterer in intralipid is approximately 100 nm.[25] The similarity of the M_{44}/M_{11} matrix elements for the cells and intralipid implies that the distribution of particle sizes is similar in both suspensions and is comprised of many small particles and a few large particles.

Cell Volume

Consistent with earlier work by other authors,[14] the average cell volume was found to be smaller for the MR1 cells than the M1 cells. This is illustrated in Figure 7, which shows representative volume distributions for M1 and MR1 cells. Analysis of volume distributions for 6 separate experiments showed that exponential-phase M1 cells had a mean volume of 1.33×10^3 μm^3 with a standard deviation of 0.127×10^3 μm^3 compared with a mean volume of 1.09×10^3 μm^3 with a standard deviation of 0.131×10^3 μm^3 for exponential phase MR1 cells. This equates to mean dimensions of 13.6 and 12.8 μm, respectively. Plateau phase cells of both cell lines were significantly smaller (mean volume = 0.871×10^3 μm^3 and standard deviation = 0.178×10^3 μm^3 for M1 vs. mean volume = 0.815×10^3 μm^3 and standard deviation = 0.060×10^3 μm^3 for MR1 [mean dimensions of 11.8 μm and 11.6 μm, respectively]).

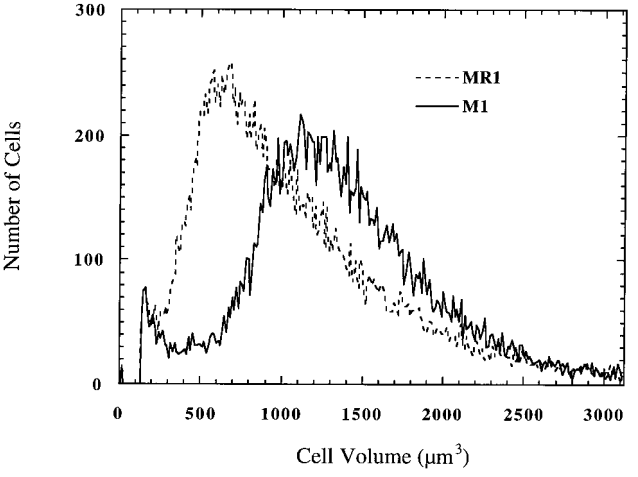

FIGURE 7. Representative cell volume distributions for exponential phase M1 and MR1 cell populations.

DISCUSSION

Three types of measurements that analyze scattering properties were conducted on M1 and MR1 cells. Elastic-scatter measurements demonstrated that there is a difference in optical properties between the M1 and MR1 cells. Measurements of $\mu_s'(\lambda)$ indicated that the difference is in the scattering rather than the absorption properties and is due to the average size of a scattering particle being larger in MR1 cells than in M1 cells. The polarization sensitive measurements of diffuse backscattering also provide strong evidence that there is a difference in the average scatterer size in the M1 and MR1 cells.

In biologic cells there are a wide variety of particles sizes ranging from proteins to organelles to the

cell itself. Therefore, it is reasonable to expect that there is distribution of scatterer sizes. Indeed, it has been shown that the spectrum of index variations is quite broad, with the power spectrum of index variations having a power-law dependence over at least one decade of spatial frequency.[26] The relative contribution of different parts of the cell to the scattering cross-section is not known and likely depends on the type of cell. For liver cells mitochondria most likely are responsible for the majority of light scattering.[27] Scattering from membrane structures also may be a significant contributor.[28]

Our data provide evidence of a change in average scatterer size between the tumorigenic MR1 cells and the nontumorigenic M1 cells. The $\mu_s'(\lambda)$ measurements and the polarization measurements show that this change is quite small, being only a few tens of nanometers. A change in the average particle size can be caused by two different effects: there could be a change in the size of the scattering particles or there could be a change in the number distribution of scattering particles. Because a gedanken experiment assumes that all the scattering is from the mitochondria and the nuclei, the average size of the scattering particles will change if the size of the nuclei or the mitochondria changes. The average size of the scattering particles also will change if there is a change in the number of mitochondria. Our data cannot differentiate between a change in the number of scatterers of a certain size or a change in the actual size of the scattering centers.

It is interesting to note that the optical measurements suggest that the scattering centers in MR1 cells are larger than those in M1 cells, yet direct measurements of cell volume showed that the M1 cells themselves were significantly larger. This implies that the size of the cell itself essentially has no effect on the scattering properties measured in this study. The light scattering centers are expected to be nuclei and other internal organelles. We believe that the nucleus contributes significantly to scattering, due to the fact that the angular distribution of scattering from nuclei is more similar to that of the cell than is the angular distribution of scattering from mitochondria.[23] Future studies will focus on determining the structural basis for the changes in light scattering.

An important issue concerns the relevance of measurements of these cell suspensions to in vivo measurements of tissue. Tumors typically arise in epithelial tissues, which contain very few fibrous structures.[29] Therefore, measurements of cells in the absence of fibrous structure is relevant. Another more important concern regarding the extrapolation of these results to in vivo measurements is the inhomogeneity of cells in tissue, particularly in tumors. For our measurements we had fairly homogenous samples. Cells in tumors will be less homogeneous for several reasons, for example, the cells will be in very different stages of growth because tumors can contain rapidly dividing cells, nonreproducing cells, and necrotic cells. Future studies are needed to address this issue. Finally, it is important to note that we have demonstrated that light scattering is sensitive to morphologic changes only in one pair of cells. Without further data regarding other systems, this information should not be interpreted as a general result.

CONCLUSIONS

Light scattering differences have been observed between cells from two consecutive stages of a multistep carcinogenesis model. The cells differed only by the addition of a *ras* oncogene that is common in many types of cancer. The changes in light scatter were measured by both wavelength-dependent and polarization-dependent methods. Both methods indicate that the difference in scattering is due to the average dimension of the scatterers being a few tens of nanometers smaller in the nontumorigenic cells compared with the tumorigenic cells. This work demonstrates the sensitivity of wavelength-dependent and polarization-dependent light scattering measurements to cell morphology and is relevant to the development of noninvasive, optical tissue diagnostic methods.

REFERENCES

1. Richards-Kortum R, Sevick-Muraca E. Quantitative optical spectroscopy for tissue diagnosis. *Annu Rev Phys Chem* 1996;47:555–606.
2. Bigio IJ, Mourant JR. Ultraviolet and visible spectroscopies for tissue diagnostics: fluorescence spectroscopy and elastic-scatter spectroscopy. *Phys Med Biol* 1997;44:803–14.
3. Ramanujam N, Mitchell MF, Mahadevan A, Thomsen S, Malpica A, Wright T, et al. Development of a multivariate statistical algorithm to analyze human cervical tissue fluorescence-spectra acquired in-vivo. *Lasers Surg Med* 1996;19: 46–62.
4. Vo-Dinh T, Panjehpour M, Overholt BF, Farris C, Buckley FP III, Sneed R. In vivo cancer diagnosis of the esophagus using differential normalized fluorescence. *Lasers Surg Med* 1995; 16:41–7.
5. Schomaker KT, Frisoli JK, Compton CC, Flotte TJ, Richter JM, Nishioka NS, et al. Ultraviolet laser-induced fluorescence of colonic tissue: basic biology and diagnostic potential. *Lasers Surg Med* 1992;12:63–78.
6. Mourant JR, Bigio IJ, Boyer J, Conn RL, Johnson T, Shimada T. Spectroscopic diagnosis of bladder cancer with elastic light scattering. *Lasers Surg Med* 1995;17:350–57.
7. Mourant JR, Bigio IJ, Boyer J, Johnson T, Lacey J. Detection of gastrointestinal cancer by elastic-scattering spectroscopy. *J Biomed Opt* 1996;1:192–99.

8. Perelman LT, Backman V, Wallace M, Zonios G, Manohoran R, Nusrat A, et al. Observation of periodic fine structure in reflectance from biological tissue: a new technique for measuring nuclear size distribution. *Phys Rev Lett* 1988;80:627–30.
9. Fishkin JB, Coquoz O, Anderson ER, Brenner M, Tromberg BJ. Frequency-domain photon migration measurements of normal and malignant tissue optical properties in a human subject. *Appl Opt* 1997;36:10–20.
10. Tearney GJ, Brezinski ME, Bouma BE, Boppart SE, Pitris C, Southern JF, et al. In vivo endoscopic optical biopsy with optica coherence tomograpy. *Science* 1997;276:2037–39.
11. Cheong W-F, Prahl SA, Welch AJ. A review of the optical properties of biological tissues. *IEEE J Quant Elect* 1990;26: 2166–85.
12. Liu H, Chance B, Hielscher AH, Jacques SL, Tittel FK. Influence of blood vessels on the measurement of hemoglobin oxygenation as determined by time-resolved reflectance spectroscopy. *Med Phys* 1995:22:1209–17.
13. Land H, Parada LF, Weinberg RA. Tumorigenic conversion of primary embryo fibroblasts requires at least two cooperating oncogenes. *Nature* 1983;304:596–602.
14. Kunz-Schughart LA, Simm A, Mueller-Klieser W. Oncogene-associated transformation of rodent fibroblasts is accompanied by large morphologic and metablic alterations. *Oncol Rep* 1995;2:651–61.
15. LaRue KA, Bradbury EM, Freyer JP. Differential regulation of cyclin dependent kinase inhibitors in monolayer and spheroid cultures of tumorigenic and nontumorigenic fibroblasts. *Cancer Res* 1998;58:1305–14.
16. Farrell TJ, Patterson MS, A diffusion theory model of spatially resolved, steady-state diffuse reflectance for the noninvasive determination of tissue optical properties. *Med Phys* 1992;19:879–888.
17. Haskell RC, Svaasand LO, Tsay T-T. Boundary conditions for the diffusion equation in radiative transfer. *J Opt Soc Am [A]* 1994;11:2727–41.
18. Hielscher AH, Eick AA, Mourant JR, Shen D, Freyer JP, Bigio IJ. Diffuse backscattering Mueller matrices for highly scattering media. *Optics Express* 1997;1:441–54.
19. Hielscher AH, Mourant JR, Bigio IJ. Influence of particle size and concentration on the diffuse backscattering of polarized light from tissue phantoms and biological cell suspensions. *Appl Opt* 1997;36:125–35.
20. Bickel WS, Bailey WM. Stokes vectors, Mueller matrices, and polarized scattered light. *Am J Phys* 1985;53:468–78.
21. Jacques SL, Gutsche A, Schwartz J, Wang L, Tittel FK. Video reflectometry to extract optical properties of tissue in vivo. In: Mueller G, Chance B, Alfano RR, Arridge SR, Beuthan J, Gratton E, et al. editors. Medical optical tomography: functional imaging and monitoring. Volume 11 of the SPIE Institute Series. Bellingham, Washington: Society of Photo-Optical Instrumentation engineers, 1992:211–26.
22. Kienle A, Lilge L, Patterson MS, Hibst R, Steiner R, Wilson BC. Spatially resolved absolute diffuse reflectance measurements for noninvasive determination of the optical scattering and absorption coefficients of biological tissue. *Appl Opt* 1996;35:2304–14.
23. Fisher JC. Photons physiatrics, and physicians: practical guide to understanding laser light interaction with living tissue. Part I. *J Clin Laser Med Surg* 1992;10:419–425.
24. Mourant JR, Freyer JP, Hielscher AH, Eick AA, Johnson TM. Mechanisms of light scattering from biological cells relevant to noninvasive optical tissue diagnostics. *Appl Opt* 1998;37: 3586–93.
25. van Staveren HJ, Moes CJM, van Marle J, Prahl SA, van Gemert MJC. Light scattering in Intralipid-10% in the wavelength range of 400-1100 nm. *Appl Opt* 1991;30:4507–14.
26. Schmitt JM, Kumar G. Turbulent nature of refractive-index variations in biological tissue. *Opt Lett* 1996;21:1310–12.
27. Beauviot B, Kitai T, Chance B. Contribution of the mitochondrial compartment to the optical properties of the rat liver: a theoretical and practical approach. *Biophys J* 1994; 67:2501–10.
28. Beuthan J, Minet O, Helfmann J, Herrig M, Muller G. The spatial variation of the refractive index of biological cells. *Phys Med Biol* 1996;41:369–82.
29. Junquiera LC, Carneiro J, Kelley RO. Basic histology. 7th edition. Norwalk: Appleton and Lange, 1992.